Self-Assembled Multilayers of Titania Nanoparticles and Nanosheets with Polyelectrolytes

Zhong-Sheng Wang, Takayoshi Sasaki,*,† Masaru Muramatsu, Yasuo Ebina, Tomohiro Tanaka, Lianzhou Wang, and Mamoru Watanabe

Advanced Materials Laboratory, National Institute for Materials Science, 1-1 Namiki, Tsukuba, Ibaraki 305-0044, Japan

Received April 30, 2002. Revised Manuscript Received October 17, 2002

Self-assembled multilayer films of titania nanoparticles and composite films of nanoparticles/nanosheets have been fabricated on various substrates using appropriate polyelectrolytes as counterions. UV−vis spectroscopy and ellipsometric data for the multilayer buildup process of TiO_2 nanoparticles indicated that a nearly equivalent amount of nanoparticles can be deposited layer-by-layer with a polyanion such as poly(sodium 4-styrene sulfonate). The average thickness of the TiO_2 nanoparticle layer was determined to be about 6.3 nm, which is in good agreement with TEM and AFM data. TiO_2 nanoparticles and $Ti_{1-\delta}O_2$ nanosheets are assembled in various sequences with appropriate polyelectrolytes sandwiched between them, which yielded novel intergrown nanoparticle/nanosheet films. Polymers between the nanoparticle and/or nanosheet layers could be decomposed by UV irradiation to yield inorganic multilayer films, which is confirmed by IR and X-ray photoelectron spectroscopy combined with Ar^+ depth profiling. Small ions such as SO_4^{2-} and NH_4^+ were resulted from polymers as counterions for the nanoparticles and nanosheets.

Introduction

The synthesis of TiO_2 nanoparticles has been the target of intensive research because of their versatility in terms of high chemical stability, excellent optical properties, and high photochemical reactivity. Nanoparticles as small as 2 nm have been synthesized by hydrolysis of titanium salts or laser ablation of bulk TiO_2, and these particles exhibit a range of useful properties suitable for applications such as photoelectrical energy conversion[1,2] and photocatalytic decomposition of pollutants or water.[3−5]

Nanosized titanium oxide can also be produced as unilamellar crystallites of composition $Ti_{1-\delta}O_2$ ($\delta \sim 0.09$).[6] This so-called nanosheet crystallite is characterized by extremely high two-dimensional anisotropy with lateral dimensions of 0.1−1 μm and thickness of ~1 nm, in sharp contrast to spherical nanoparticles.[7] The atomic architecture is of γ-FeOOH type which is different from the crystal structure of anatase and rutile that most TiO_2 nanoparticles adopt.[8] As a reflection of the molecular thickness, the nanosheets exhibit a sharp and intense absorption peak at 265 nm that is significantly blue-shifted from the absorption edge of bulk TiO_2.[9] These optical features are clearly distinctive from those of TiO_2 nanoparticles.

Considerable effort has been devoted to the fabrication of titania thin films for the above-mentioned practical applications of these important materials. Recent technological progress requires development of ultrathin films with highly sophisticated functionalities. To satisfy this demand, it is of essential importance to achieve precise control of the film architecture on the nanometer-scale. Self-assembly via sequential adsorption of oppositely charged polyelectrolytes[10] is an effective route for the layer-by-layer construction of nanostructured films.[11] Several groups have reported the fabrication of multilayer films of TiO_2 nanoparticles and organic polymers via electrostatic self-assembly.[12−16] Regular film growth has been discussed on the basis of UV−vis spectra and ellipsometric thickness data. On the other hand, we have recently demonstrated that $Ti_{1-\delta}O_2$ nanosheets can be assembled alternately with a polycation to yield a multilayer film.[17]

* Corresponding author. E-mail: sasaki.takayoshi@nims.go.jp. Fax: +81-298-54-9061.

† CREST, Japan Science and Technology Corporation (JST).

(1) (a) O'Regan, B.; Grätzel, M. *Nature* (London) **1991**, *353*, 737. (b) Hagfeldt, A.; Grätzel, M. *Chem. Rev.* **1995**, *95*, 49.

(2) (a) Wang Z.-S.; Li, F.-Y.; Huang, C.-H.; Wang, L.; Wei, M.; Jin, L.-P.; Li, N.-Q. *J. Phys. Chem. B* **2000**, *104*, 9676. (b) Wang Z.-S.; Li, F.-Y.; Huang, C.-H. *Chem. Commun.* **2000**, 2063. (c) Wang Z.-S.; Li, F.-Y.; Huang, C.-H. *J. Phys. Chem. B* **2001**, *105*, 9210.

(3) Fujishima, A.; Honda, K. *Nature* **1972**, *238*, 37.

(4) Sato, S.; White, J. M. *Chem. Phys. Lett.* **1980**, *72*, 83.

(5) Kawai, T.; Sakata, T. *Nature* **1980**, *286*, 474.

(6) (a) Sasaki, T.; Watanabe, M.; Hashizume, H.; Yamada, H.; Nakazawa, H. *J. Am. Chem. Soc.* **1996**, *118*, 8329. (b) Sasaki, T.; Watanabe, M. *J. Am. Chem. Soc.* **1998**, *120*, 4682.

(7) Sasaki, T.; Ebina, Y.; Kitami, Y.; Watanabe, M.; Oikawa, T. *J. Phys. Chem. B* **2001**, *105*, 6116.

(8) Sasaki, T.; Watanabe, M.; Michiue, Y.; Komatsu, Y.; Izumi, F.; Takenouchi, S. *Chem. Mater.* **1995**, *7*, 1001.

(9) Sasaki, T.; Watanabe, M. *J. Phys. Chem. B* **1997**, *101*, 10159.

(10) Decher, G. *Science* **1997**, *277*, 1232.

(11) Wang Z.-S.; Huang, C.-H.; Li, F.-Y.; Weng, S.-F.; Ibrahim, K.; Liu, F.-Q. *J. Phys. Chem. B* **2001**, *105*, 4230.

(12) Cassagneau, T.; Fendler, J. H.; Mallouk, T. E. *Langmuir* **2000**, *16*, 241.

(13) Liu, Y.; Wang, A.; Claus, R. *J. Phys. Chem. B* **1997**, *101*, 1385.

(14) Kovtyukhova, N.; Ollivier, P. J.; Chizhik, S.; Dubravin, A.; Buzaneva, E.; Gorchinskiy, A.; Marchenko, A.; Smirnova, N. *Thin Solid Films* **1999**, *337*, 166.

(15) Rouse, J. H.; Ferguson, G. S. *Adv. Mater.* **2002**, *14*, 151.

(16) Sun, Y.; Hao, E.; Zhang, X.; Yang, B.; Shen, J.; Chi, L.; Fuchs, H. *Langmuir* **1997**, *13*, 5168.

10.1021/cm0204268 CCC: $25.00
Published on Web 01/22/2003

As TiO_2 nanoparticles can be prepared in various sizes and qualities with respect to structure and crystallinity, the resulting multilayer films should have physical properties that are related to the nature of nanoparticles. From this point of view, further work on the fabrication of nanoparticle films will be necessary to acquire a deeper understanding of the films. In addition, it would be of great interest to synthesize a heterocomposite film incorporating both nanoparticles and nanosheets. The very different morphologies, crystal structures, and properties of them may lead to new physicochemical properties for such composite films. The present study deals with the fabrication of multilayer films of TiO_2 nanoparticles and polyanions, and novel composite films composed of nanoparticles and nanosheets with appropriate polyelectrolytes.

Experimental Section

Materials. Poly(sodium 4-styrene sulfonate) (PSS), polyethylenimine (PEI), 50 wt % aqueous solutions, and poly (diallyldimethylammonium chloride) (PDDA), 20 wt % aqueous solution, were purchased from Aldrich Co. and used without further purification. Molecular weight is $\sim 7.5 \times 10^5$ for PEI, $1 \times 10^5 - 2 \times 10^5$ for PDDA, and $\sim 7 \times 10^4$ for PSS. All water used was purified to a resistivity of greater than 17 MΩ cm by passing through a Millipore Milli-Q membrane filtration system. All other solvents and chemicals were of reagent grade.

A colloidal suspension of $Ti_{1-\delta}O_2^{4\delta-}$ ($\delta \sim 0.09$) nanosheets (denoted $Ti_{1-\delta}O_2$) was synthesized by delaminating a layered titanate, $H_{0.7}Ti_{1.825}\square_{0.175}O_4 \cdot H_2O$ (□: vacancy), into single layers.[6,8] Cs-titanate $Cs_{0.7}Ti_{1.825}\square_{0.175}O_4$ was prepared by heating an intimate mixture of Cs_2CO_3 and TiO_2 at 1000 °C, followed by treatment with 1 mol dm^{-3} HCl solution. The resulting acid-exchanged form (1 g), $H_{0.7}Ti_{1.825}\square_{0.175}O_4 \cdot H_2O$, was shaken with 250 cm^3 of 0.017 mol dm^{-3} tetrabutylammonium hydroxide (TBAOH) solution for 10 d.

TiO_2 nanoparticles (denoted TiO_2) in suspension (STS-100, pH 1.5, 20 wt % aqueous suspension) was obtained as a gift from Ishihara Sangyo Kaisha, Ltd. Transmission electron microscopy (TEM) observations revealed that the suspension contained monodisperse nanoparticles in single-crystal quality (anatase) with average dimensions of 6.2 ± 0.8 nm (standard deviation).

Fabrication of Self-Assembled Films. Quartz glass platelets and silicon wafers were used as substrates after they were cleaned by immersion in a bath of 1:1 methanol/HCl and concd H_2SO_4 for 30 min each. A PEI solution (1.25 g dm^{-3}) and the $Ti_{1-\delta}O_2$ suspension (0.08 g dm^{-3}) were added with a dilute HCl solution to adjust their pH to 9, while a PDDA solution (20 g dm^{-3}) containing 0.5 mol dm^{-3} NaCl was added with a TBAOH solution to make its pH 9. A PSS (7 g dm^{-3}) solution was prepared by dissolving a weighed amount of PSS in a HCl solution having a pH of 1.5. TiO_2 nanoparticle suspensions (0.001−0.36 g dm^{-3}) were prepared by diluting the parent one with a HCl solution (pH 1.5). It is important to keep the pH value of TiO_2 nanoparticle suspensions below 2 to avoid deterioration of the nanoparticles. Substrates were precoated with a thin PEI layer by dipping them in a PEI solution for 20 min. The substrate surface became positively charged through this procedure.

Ultrathin films of PSS and TiO_2 nanoparticles, $(PSS/TiO_2)_n$, were prepared by repeating the following steps on the substrate *n* times: (1) immersing in the PSS solution for 20 min; (2) washing with HCl solution (pH 1.5); (3) immersing in TiO_2 suspension for 20 min; (4) washing with HCl solution (pH 1.5) followed by drying under N_2 gas flow.

Composite assemblies of nanoparticles and nanosheets were fabricated by a similar sequential deposition. PDDA was used as a self-assembly counterpart for the titania nanosheets, $Ti_{1-\delta}O_2$, and PSS was combined with TiO_2 nanoparticles. The film was washed with HCl solution (pH 1.5) in the assembly process of the nanoparticle layer, and with Milli-Q water in the process of nanosheet deposition.

Instrumentation. A 500-W Xe lamp (San-ei Electric, XEF-501S) was used to expose the films to UV light. The lamp emitted UV light continuously from 230 to 800 nm centered around 400 nm, about 90% photons of which fall into the range of 230 to 500 nm. The sample was placed 10 cm from the light source and irradiated for 3 d. An integrated light intensity under this arrangement was ~2.5 mW cm^{-2}, which was measured with a spectroradiometer (USR-30 Ushio Denki). UV−vis absorption and reflectance spectra were recorded on a Hitachi U-4000 spectrophotometer. FT-IR spectra for self-assembled films on Si wafers (5×6 cm^2) were measured in transmission mode at a Brewster's angle of 75° using a Digilab S-45 FT-IR spectrometer. X-ray photoelectron spectra (XPS) were collected at a takeoff angle of 45° using a Physical Electronics XPS-5700 spectrometer with Al Kα X-ray line (1486.6 eV). The vacuum inside the spectrometer during analysis was $\sim 10^{-7}$ Pa. Etching of the films for depth profiling was performed using Ar^+ from a gun (3.00 kV). The sputtering rate used is comparable to be 0.96 nm/min for SiO_2.

A Seiko SPA 400 atomic force microscopy (AFM) system was used to examine the surface topography of the films prepared on Si wafers. AFM images were acquired in tapping mode using a Si tip cantilever with a force constant of 20 N cm^{-1}.

Film thickness was monitored using a Jovin-Ybon UVISEL/DH10 spectroscopic ellipsometer. Typically, the thickness was measured in 10 different locations and averaged. Optical constants for a Si wafer and multilayer films were determined as described previously.[17b] Refinements indicated thicknesses of 0.80 and 0.51 nm for PEI and PSS layers, respectively.

TEM observations were performed on a JEM 1010 electron microscope operating at an accelerating voltage of 100 kV.

Results and Discussion

Formation of Multilayer Films of TiO_2 Nanoparticles. TiO_2 colloidal particles are amphoteric;[18] whether the particle surface is positively or negatively charged depends on the pH of surrounding media. As TiO_2 nanoparticles are positively charged in acidic media, we selected a polyanion, PSS, as a counterpart for self-assembly.

The concentration of TiO_2 suspension and the deposition duration are two important factors for adsorption of nanoparticles and eventually for fabrication of a multilayer assembly with a well-ordered nanoarchitecture. Figure 1 shows the UV absorbance of the PSS/TiO_2 bilayer deposited on a quartz glass substrate as a function of the concentration of titania nanoparticle suspension for a fixed deposition time of 20 min. The absorbance increased with the concentration of the TiO_2 nanoparticle suspension up to 0.2 g dm^{-3}. The absorbance (228 nm) is mainly attributable to TiO_2 nanoparticles as described below, indicating that this tendency represents an increase in the absorption of nanoparticles with increasing suspension concentration. On the other hand, a plateau was reached at above 0.2 g dm^{-3}, indicating a saturation of adsorption. The effect of dipping duration was also examined using the TiO_2 suspension at 0.2 g dm^{-3}, revealing that saturation with

(17) (a) Sasaki, T.; Ebina, Y.; Watanabe, M.; Decher, G. *Chem. Commun*. **2000**, 2163. (b) Sasaki, T.; Ebina, Y.; Tanaka, T.; Harada, M.; Watanabe, M. *Chem. Mater*. **2001**, *13*, 4661.

(18) Isoelectric point is 6.2. Ring, Terry A. *Fundamentals of Ceramic Powder Processing and Synthesis*; Academic Press: San Diego, CA, 1996.

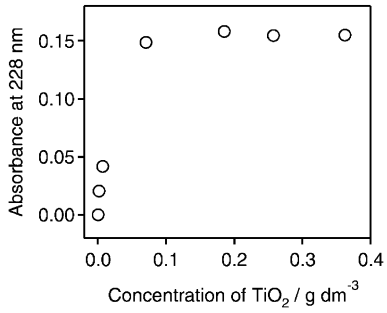

Figure 1. Relationship between absorbance at 228 nm of PSS/TiO_2 bilayer and concentration of TiO_2 nanoparticles (deposition time 20 min).

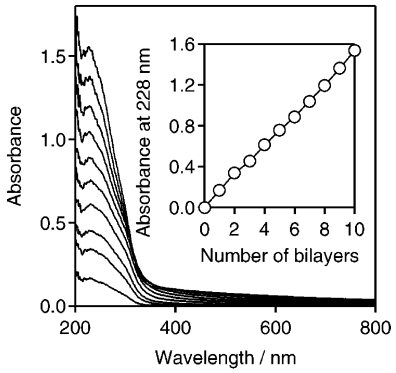

Figure 2. UV−vis absorption spectra for $(PSS/TiO_2)_{10}$ multilayers. Nanoparticle concentration of 0.2 g dm^{-3} and deposition time of 20 min were employed in the film fabrication. A plot of absorbance at 228 nm vs the number of bilayers (inset).

similar absorbance was attained after about 20 min. No noticeable increment in absorbance was observed with either increasing concentration above 0.2 g dm^{-3} or prolonging deposition time longer than 20 min. We therefore employed these experimental conditions in the fabrication of PSS/TiO_2 multilayer films.

The growth of self-assembled $(PSS/TiO_2)_n$ multilayers was monitored by measuring their UV−vis absorption spectra immediately after each deposition cycles (Figure 2). The UV-absorption features are attributable to TiO_2 nanoparticles and PSS. An average increment in absorbance of 0.155 per bilayer at 228 nm is the sum of 0.024 due to the PSS layer and 0.131 for the TiO_2 nanoparticle layer.[19] The good linearity (inset of Figure 2) between absorbance and the number of bilayers indicates that each layer of nanoparticles contributes a nearly equal amount of TiO_2 to the thin film. The linearity obtained is better and the absorbance enhancement per TiO_2 deposition is higher compared to the previously reported data for similar multilayer films of TiO_2 nanoparticles.[12−14]

The thickness of $(PSS/TiO_2)_n$ multilayer films determined by spectroscopic ellipsometry also provided strong evidence for the success of layer-by-layer deposition (Figure 3). The ellipsometric thickness grew linearly with the number of PSS/TiO_2 bilayers, and the average thickness of each PSS/TiO_2 bilayer was 6.8 ± 0.3 nm,

(19) Contribution of PSS layer to the absorbance at 228 nm, 0.024, was estimated from the data for two films such as PEI/PSS and PEI/PSS/TiO_2/PSS. A film did not grow efficiently once dried after adsorption of PSS layer, whereas it grew well even though dried after nanoparticle deposition. Therefore, we did not measure the absorbance increase after deposition of PSS.

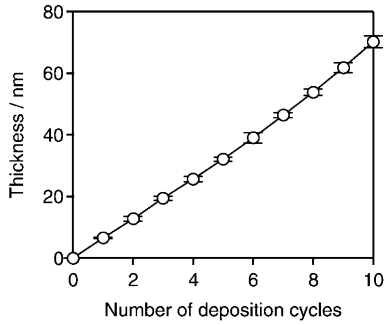

Figure 3. Ellipsometric thickness plots for $(PSS/TiO_2)_n$. Error bar represents three times standard deviation.

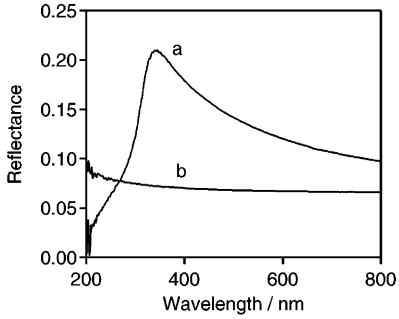

Figure 4. Reflectance spectra for (a) the multilayer film of $(PSS/TiO_2)_{10}$ on quartz glass and (b) bare quartz glass substrate.

consisting of 0.5 ± 0.1 nm of PSS and 6.3 ± 0.2 nm of the TiO_2 nanoparticles. The latter dimension is in excellent accordance with the diameter of nanoparticles (6.2 ± 0.8 nm) determined by TEM.

It is important to know how densely TiO_2 nanoparticles are packed in the layer. This can be roughly estimated from the optical data by applying the formulation described in our recent report on a multilayer of titania nanosheets and polycations.[17b] The suspension of TiO_2 nanoparticle exhibited Lambert−Beer behavior, giving a molar extinction coefficient, ϵ, of 6.74×10^3 mol^{-1} dm^3 cm^{-1} at 228 nm. A self-assembled film with 10 layer pairs on both sides of the quartz glass substrate had an apparent absorbance of 1.31 at 228 nm (Figure 2), corresponding to a transmittance of 0.049. Due to film reflectance, the actual absorption should be lower than the observed value according to

$$T = 1 - R - A \qquad (1)$$

where T and R are the transmittance and reflectivity and A is the damping ratio due to actual absorption. The reflectance spectrum (Figure 4) of the same 10-layered film gave a reflectivity of 0.047 at 228 nm. Consequently, A in eq 1 is 0.904 (= 1 − 0.047 − 0.049), which can be converted to an absorbance of 1.02. The average absorbance per TiO_2 layer can then be calculated to be 0.051 (= $^{1.02}/_{20}$). This absorbance corresponds to 6.05×10^{-7} g cm^{-2} of adsorbed nanoparticles on the basis of the molar extinction coefficient of the TiO_2 nanoparticle suspension. Here, to the first approximation, we take the extinction coefficient of TiO_2 suspension as that for the nanoparticle film.

If we consider a perfect monolayer of TiO_2 nanoparticles hexagonally close-packed, one nanoparticle is accommodated in a two-dimensional unit cell, the

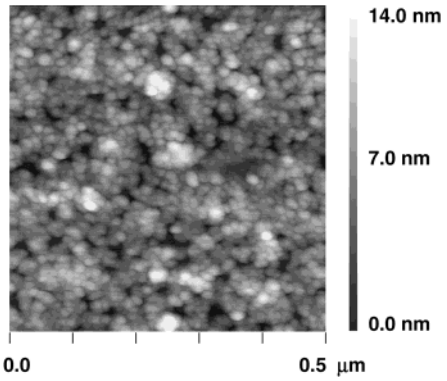

Figure 5. Tapping-mode AFM image of the first TiO_2 nanoparticle layer on a Si wafer (as-grown).

area (S_{uc}) of which is given by

$$S_{uc} = d^2 \sin 120° \quad (2)$$

where d is the nanoparticle diameter. Assuming the substrate is completely covered with such a monolayer of 6.2-nm TiO_2 nanoparticles, the weight (m) of the monolayer is 1.46×10^{-6} g cm^{-2} as calculated from

$$m = \frac{4}{3}\pi r^3 \rho / S_{uc} \quad (3)$$

where r is the radius (3.1 nm) of the nanoparticle, and $\rho = 3.89$ g cm^{-3} is the density of anatase TiO_2. Comparison of this value with that derived from the optical data gives a surface coverage of ~42% (= $(6.05 \times 10^{-7})/(1.46 \times 10^{-6})$). This relatively low coverage may be reasonable because strong electrostatic repulsion between positively charged nanoparticles is expected.

The tapping-mode AFM image (Figure 5) revealed that the average height of nanoparticles was 7.0 ± 1.0 nm, which is in agreement with the ellipsometric and TEM data. The substrate surface appears to be densely covered with nanoparticles. However, it should be noted that the probe size of the Si cantilever (2−5 nm diam.) is comparable to the nanoparticle size, resulting in spurious enlargement of each nanoparticle. In the case of a close-packed arrangement of 6.2-nm nanoparticles, 300 nanoparticles can be expected per 100×100 nm^2 area. In contrast, only 100 particles or less were actually observed, although the poorly resolved image prevented precise counting. This may rather be compatible with the discussion on surface coverage on the basis of the optical data.

Alternate Self-Assembly of TiO_2 Nanoparticles and $Ti_{1-\delta}O_2$ Nanosheets. In contrast to TiO_2 nanoparticles, $Ti_{1-\delta}O_2$ nanosheets are inherently negatively charged[6] due to the vacancies at Ti positions. We have already reported the multilayer assemblies of nanosheets with polycations,[17] and here we demonstrate that heterocomposite films of nanoparticles/nanosheets can be constructed by assembling trilayers of PDDA/PSS/TiO_2 and PSS/PDDA/$Ti_{1-\delta}O_2$ in various sequences. Figure 6(a) and (b) shows the UV−vis absorption spectra for layer-by-layer assembly of nanoparticles and nanosheets in two different alternations. The optical features attributable to nanoparticles and nanosheets appeared as a simple sum of each trilayer component for PDDA/PSS/TiO_2 and PSS/PDDA/$Ti_{1-\delta}O_2$. The regular enhancement

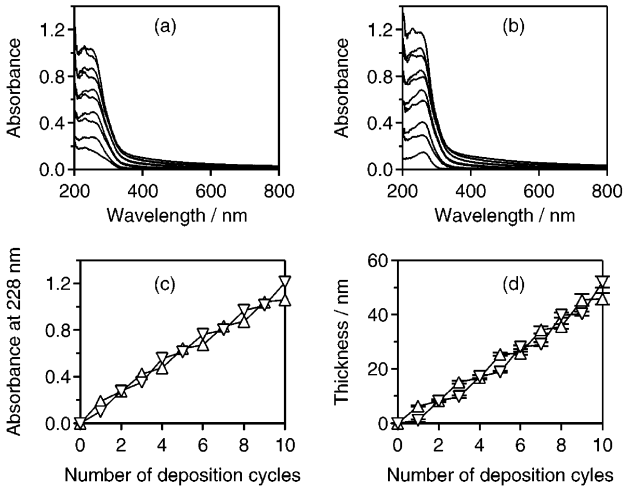

Figure 6. UV−vis absorption spectra for multilayer composite film of (a) PSS/TiO_2/PSS/PDDA/$Ti_{1-\delta}O_2$/(PDDA/PSS/TiO_2/PSS/PDDA/$Ti_{1-\delta}O_2)_{n-1}$ and (b) $Ti_{1-\delta}O_2$/PDDA/PSS/TiO_2/(PSS/PDDA/$Ti_{1-\delta}O_2$/PDDA/PSS/$TiO_2)_{n-1}$. (c) Plot of absorbance at 228 nm vs the number of bilayers. (d) Ellipsometric thickness against the number of deposition cycles. (△) PSS/TiO_2/PSS/PDDA/$Ti_{1-\delta}O_2$/(PDDA/PSS/TiO_2/PSS/PDDA/$Ti_{1-\delta}O_2)_{n-1}$. (▽) $Ti_{1-\delta}O_2$/PDDA/PSS/TiO_2/(PSS/PDDA/$Ti_{1-\delta}O_2$/PDDA/PSS/$TiO_2)_{n-1}$. Error bar represents three times standard deviation.

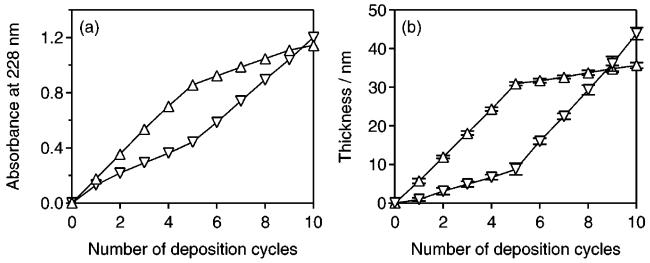

Figure 7. (a) Absorbance at 228 nm and (b) ellipsometric thickness as a function of the number of deposition cycles: (△) $(PSS/TiO_2)_n$/PSS/$(PDDA/Ti_{1-\delta}O_2)_n$; (▽) $(Ti_{1-\delta}O_2/PDDA)_n$/$(PSS/TiO_2)_n$. Error bar represents three times standard deviation.

as seen in Figure 6(c) indicates successful intergrowth of nanoparticles and nanosheets. The average increases in absorbance for trilayer deposition of PDDA/PSS/TiO_2 and PSS/PDDA/$Ti_{1-\delta}O_2$, 0.17 (at 228 nm for nanoparticles) and 0.10 (at 265 nm for nanosheets), were comparable to those observed for the multilayer buildup process of each trilayer, PDDA/PSS/TiO_2 and PSS/PDDA/$Ti_{1-\delta}O_2$, alone. Ellipsometry measurements provide additional evidence as illustrated in Figure 6(d): a nearly constant increase in film thickness was obtained, ~6.8 nm for the bilayer of PSS/TiO_2 and ~1.8 nm for that of PDDA/$Ti_{1-\delta}O_2$. The film growth rates were again similar to those observed for multilayers of nanoparticles and nanosheets individually.[17b]

Nanoparticles and nanosheets can be deposited in many different sequences, as shown by the extreme examples in Figure 7. In the fabrication of $(PSS/TiO_2)_5$-PSS/$(PDDA/Ti_{1-\delta}O_2)_5$, absorbance at 228 nm increased linearly but with different slopes. A larger slope was observed for the first 5 bilayers of PSS/TiO_2 whereas a smaller slope was evident for the following 5 bilayers of PDDA/$Ti_{1-\delta}O_2$ (Figure 7(a)). Similar regularity was observed with respect to ellipsometric thickness (Figure 7(b)). A near mirror image was obtained for film deposition in the opposite sequence.

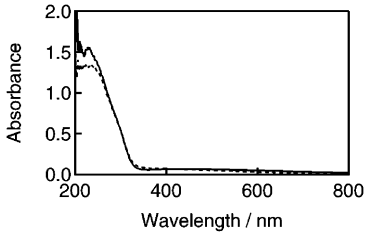

Figure 8. UV−vis absorption spectra for as-grown (PSS/TiO_2)$_{10}$ multilayers (solid line) and its UV-irradiated one (dashed line).

Theoretically, the total absorbance or thickness of a film should not be dependent on deposition sequence, but this was not the case. The film with a starting layer of nanosheet is thicker and has higher absorbance than its counterpart with a starting layer of nanoparticles (Figures 6 and 7). The surface of the nanosheet layer is much flatter than that of the nanoparticle layer and is expected to facilitate subsequent growth.

Photocatalytic Removal of Polymer. Titanium dioxide nanoparticles are well-known for their photocatalytic properties.[3−5] On the other hand, several layered metal oxides have been demonstrated to photodecompose water efficiently.[20−23] In titanium dioxide, electron−hole pairs are generated through excitation with UV light, and the holes residing in the valence band of TiO_2 have high oxidative activity. Most recently, we have demonstrated that a multilayer film of (PDDA/$Ti_{1-\delta}O_2$)$_{10}$ can be converted into a polymer-free inorganic film upon exposure to UV light.[24] In the present study, we examined removal of polymer from films containing nanoparticles and/or nanosheets. One can see from Figure 8 that the absorbance at 228 nm decreased by ~0.23 upon UV irradiation, which is comparable to the total absorbance at the same wavelength of 10-layer PSS on both sides of the quartz glass substrate. This reduction of UV-absorbance is strong evidence for the decomposition of PSS. As will be described below, SO_4^{2-} ions are formed from PSS, but they do not have appreciable optical absorption at this wavelength.

FT-IR spectra (Figure 9) were obtained in order to clarify the changes in ultrathin films before and after irradiation based on information on the major groups in the polymers. Here, we chose films of (PSS/TiO_2)$_{10}$ and PSS/TiO_2/PSS/PDDA/$Ti_{1-\delta}O_2$/(PDDA/PSS/TiO_2/PSS/PDDA/$Ti_{1-\delta}O_2$)$_4$ as examples to discuss the changes in the IR peaks (see Supporting Information for detailed assignments). The as-grown (PSS/TiO_2)$_{10}$ film exhibited characteristic absorption bands of PSS and H_2O; relatively sharp bands at 2960, 2930, and 2851 cm^{-1} are assignable to stretching vibrations of CH_3− and −CH_2− groups, and one at 1455 cm^{-1} is due to the bending mode. Peaks at 1607 cm^{-1} for stretching of −C═C− and 1130 and 1007 cm^{-1} for bending of C−H are attributable to aromatic rings.[25] Signals due to H_2O were detected as broad bands around 3470 and 3215 cm^{-1} (stretching)

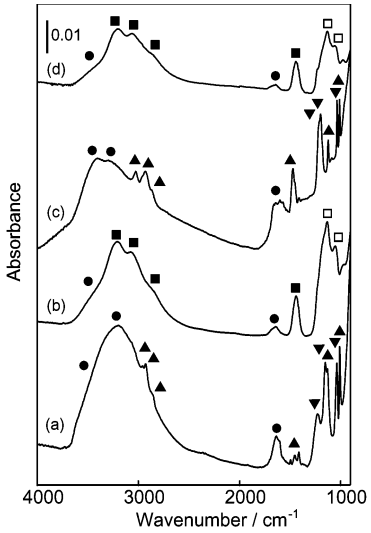

Figure 9. FT-IR spectra for (a) as-grown (PSS/TiO_2)$_{10}$ film and (b) after UV irradiation, and (c) as-grown composite film of PSS/TiO_2/PSS/PDDA/$Ti_{1-\delta}O_2$/(PDDA/PSS/TiO_2/PSS/PDDA/$Ti_{1-\delta}O_2$)$_4$ and (d) after UV-irradiation. Closed circles, triangles, inverted triangles, closed squares, and open squares indicate IR peaks for H_2O, CH_3−, −CH_2−, and Ar−H groups in polymer, $-SO_3^-$ group in PSS, NH_4^+ ions, and SO_4^- ions, respectively.

and 1633 cm^{-1} (bending).[25] The band at 1228 and 1034 cm^{-1} and the shoulder band at 1152 cm^{-1} are diagnostic of asymmetric and symmetric vibrations of $-SO_3^-$ group,[26,27] respectively. The composite film exhibited a similar spectrum. However, upon exposure to UV light, all peaks due to organic species disappeared, indicating that polymers might be eliminated to yield interesting inorganic films, which will be discussed further by the following XPS analysis.

It is interesting to explore what species were formed upon degradation of the polymer. After irradiation with UV light, the peaks of the asymmetric and symmetric stretching vibration of $-SO_3^-$ disappeared, and new strong peaks at 1132 and 1054 cm^{-1} with a shoulder appeared. These new bands may be assigned to SO_4^{2-},[26,27] suggesting PSS was decomposed to SO_4^{2-} ions under irradiation to act as counterions for positively charged nanoparticles.

In addition, the formation of NH_4^+ is indicated by three broad peaks at 3198, 3061, and 2859 cm^{-1} and a strong band at 1439 cm^{-1}. The former three are assignable to the stretching mode of NH_4^+ and the latter is attributed to the deformation vibration.[25,26] We have already demonstrated that UV treatment on the multilayer film of PDDA/$Ti_{1-\delta}O_2$ yields NH_4^+ ions as a fragment of PDDA to maintain charge neutrality with the negatively charged nanosheets.[24] It is noted that NH_4^+ was also detected upon UV irradiation of a multilayer system of PSS/TiO_2 nanoparticles. NH_4^+ could only be formed from the PEI used for priming the substrate. Thus, they are likely to be present at the film/substrate interface.

(20) Sato, S.; White, J. M. *J. Catal.* **1981**, *69*, 128.
(21) Ikeda, S.; Hara, M.; Kondo, J. N.; Domen, K. *Chem. Mater.* **1998**, *10*, 72.
(22) Ebina, Y.; Tanaka, A.; Kondo, J. N.; Domen, K. *Chem. Mater.* **1996**, *8*, 2534.
(23) Ebina, Y.; Sasaki, T.; Harada, M.; Watanabe, M. *Chem. Mater.* **2002**, *14*, 4390.
(24) Sasaki, T.; Ebina, Y.; Fukuda, K.; Tanaka, T.; Harada, M.; Watanabe, M. *Chem. Mater.* **2002**, *14*, 3524.
(25) Socrates, G. *Infrared Characteristic Group Frequencies*, 2nd ed.; Wiley & Sons Ltd: Baffins Lane, Chichester, U.K., 1994.
(26) Nyquist, R. A.; Kagel, R. O. *Infrared Spectra of Inorganic Compounds*; Academic Press: New York, 1971.
(27) Farmer, V. C. *The Infrared Spectra of Minerals*; Bartholomew Press: Dorking, Surrey, U.K., 1974.

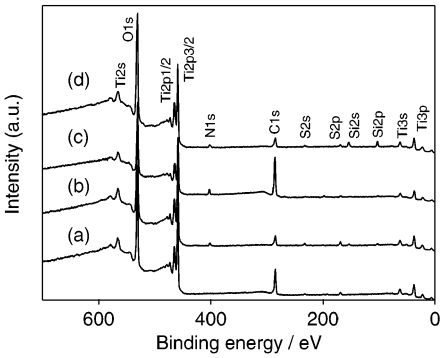

Figure 10. Survey XPS spectra for (a) as-grown $(PSS/TiO_2)_{10}$ film and (b) after UV irradiation, and (c) as-grown film of PSS/TiO_2/PSS/PDDA/$Ti_{1-\delta}O_2$/(PDDA/PSS/TiO_2/PSS/PDDA/$Ti_{1-\delta}O_2)_4$ and (d) after UV irradiation.

IR data for the composite film after UV-irradiation indicated the formation of NH_4^+ and SO_4^{2-}, similar to the case for the PSS/TiO_2 film. However, in this case, NH_4^+ and SO_4^{2-} are present in the composite film as counterions for the nanosheets and nanoparticles, respectively.

To obtain further information on changes induced by UV irradiation, XPS studies were carried out. Figure 10 shows the survey XPS spectra for the corresponding multilayer films. The as-grown films exhibited peaks assignable to Ti (458.3 eV for $2p_{3/2}$ and 464.8 eV for $2p_{1/2}$), C (285.3 eV for 1s), N (403.1 eV for 1s, composite film), S (232.1 eV for 2s and 168.7 eV for 2p), and O (530.4 eV for 1s).

For $(PSS/TiO_2)_{10}$ film, nitrogen from PEI was not detected before UV-illumination. Because the detectable depth of XPS is in the range of several nanometers, 10 layers of PSS prevent probing the priming layer of PEI at the bottom. On the other hand, a signal for N1s (401.7 eV) was observed after UV illumination. This may be ascribed to the removal of PSS. Detection of Si from the substrate can also be accounted for by this reason. For PSS/TiO_2/PSS/PDDA/$Ti_{1-\delta}O_2$/(PDDA/PSS/TiO_2/PSS/PDDA/$Ti_{1-\delta}O_2)_4$, nitrogen was detected in both the as-prepared film and the irradiated film. The primary peak for nitrogen shifted from 403.1 to 401.8 eV upon UV irradiation, the former representing a quaternary ammonium group in PDDA and the latter corresponding to NH_4^+[28] as a result of photoinduced splitting of PDDA. The binding energy at 168.2 eV assigned to sulfur in phenyl sulfonate shifted to 168.7 eV upon treatment of the films under UV light, consistent with the formation of sulfate.[28]

Compared with the as-grown films, the C1s peak weakened considerably upon UV illumination, suggesting the loss of organic polyelectrolytes. The C signal observed in the UV-treated film may be due to the carbon contamination. Such a C1s signal due to contamination has been reported in the literatures.[29] Furthermore, high-resolution XPS spectra clearly indicate the shift in binding energy for C1s and N1s (see Supporting Information), being compatible with the polymer degradation. To verify that this C signal is indeed ascribed to carbon contamination, XPS depth profiles were recorded. Figure 11 shows the typical data for the as-grown (a) and UV-treated (b) composite film. In the as-grown film, the C concentration decreased sharply within 1 min of sputtering. Afterward, the Ti, O, and C concentrations remained almost constant. In the UV-treated film, the C concentration dropped to practically zero after 1 min of sputtering while the Ti and O concentrations remained constant. These results strongly suggest adventitious carbon contamination at the very top of the film. We can conclude that exposure to UV light decomposes the organic polyelectrolyte inside the multilayers, yielding polymer-free inorganic films. Small counterions such as SO_4^{2-} and NH_4^+ are formed to keep the charge neutrality of the total system. In particular, the polymer-free composite film may be regarded as a pillared layer system composed solely of titania components.

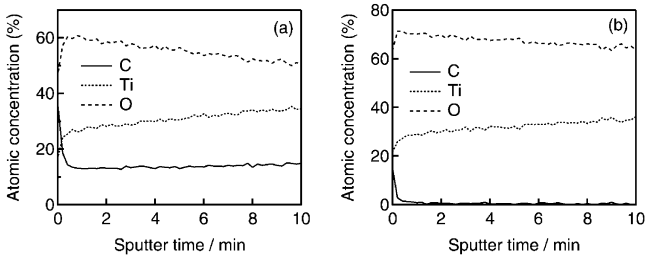

Figure 11. XPS depth profile for (a) as-grown film of PSS/TiO_2/PSS/PDDA/$Ti_{1-\delta}O_2$/(PDDA/PSS/TiO_2/PSS/PDDA/$Ti_{1-\delta}O_2)_4$ and (b) after UV irradiation.

Acknowledgment. We thank Mr. Keiji Kurashima for his kind help with TEM observations to evaluate the size of TiO_2 nanoparticles.

Supporting Information Available: High-resolution XPS and FT-IR data for the multilayer films before and after UV irradiation (PDF). This material is available free of charge via the Internet at http://pubs.acs.org.

Note Added after ASAP Posting. This article was released ASAP on 1/22/2003 with an error in the corresponding author's affiliation information. The correct version was posted on 1/28/2003.

CM0204268

(28) (a) Moulder, J.; Stickle, W.; Sobol, P.; Bomben, K. *Handbook of X-ray Photoelectron Spectroscopy*; Chastain, J., Ed; Perkin-Elmer Corp.: Eden Pairie, MN, 1992. (b) *NIST X-ray Photoelectron Spectroscopy Database*; U.S. Secretary of Commerce, U.S. Government Printing Office: Washington, DC, 1997.

(29) Swift, P.; Shuttleworth, D.; Seah, M. P. *Practical Surface Analysis by Auger and X-ray Photoelectron Spectroscopy*; Briggs, D., Seah, M. P., Eds.; John Wiley & Sons: Chichester, U.K., 1983.